Multi-Constellation Blind Beacon Estimation, Doppler Tracking, and Opportunistic Positioning with OneWeb, Starlink, Iridium NEXT, and Orbcomm LEO Satellites

Sharbel Kozhaya, Haitham Kanj, and Zaher M. Kassas
Department of Electrical and Computer Engineering
The Ohio State University, Columbus, OH, USA
kozhaya.1@osu.edu, kanj.7@osu.edu, zkassas@ieee.org

***Abstract*—A novel blind spectral approach is proposed for blind beacon estimation, Doppler tracking, and opportunistic positioning with unknown low Earth orbit (LEO) satellite signals. The framework is agnostic to the modulation and multiple access scheme adopted by LEO satellites. First, an analytical derivation of the received signal frequency spectrum is presented, which accounts for the highly dynamic channel between the LEO satellite and a terrestrial receiver. Second, a frequency domain-based blind Doppler discriminator is proposed. Third, a Kalman filter (KF)-based Doppler tracking algorithm is developed. Fourth, a blind beacon estimation framework for LEO satellites is proposed and its convergence properties are studied. Simulation results are presented showing successful beacon estimation and Doppler tracking of Starlink LEO satellites transmitting 5G orthogonal division multiple access (OFDM) signals. Experimental results are presented demonstrating the efficacy of the proposed framework on multi-constellation LEO satellites, namely OneWeb, Starlink, Orbcomm, and Iridium NEXT. Despite adopting different modulation and multiple access transmission schemes, the proposed framework is capable of successfully estimating the beacon and tracking the Doppler, in a blind fashion, of 8 LEO satellites (2 OneWeb, 4 Starlink, 1 Iridium NEXT, and 1 Orbcomm) over a period of about 560 seconds with Hz-level accuracy. The produced Doppler measurements were fused through a nonlinear least-squares estimator to localize a stationary receiver to an unprecedented level of accuracy. Starting with an initial estimate about 3,600 km away, a final three-dimensional (3–D) position error of 5.8 m and 2–D position error of 5.1 m was achieved. Aside from achieving this unprecedented accuracy, these results represent the first successful opportunistic tracking of unknown OneWeb LEO signals and their exploitation for positioning.**

***Index Terms*—Positioning, navigation, signals of opportunity, blind Doppler tracking, low Earth orbit satellite, OneWeb.**

I. Introduction

Navigation from low Earth orbit (LEO) will usher a new era for positioning, navigation, and timing (PNT). Megaconstellations of LEO satellites are being born (e.g., Starlink, OneWeb, and Kuiper), joining existing LEO constellations (e.g., Orbcomm, Globalstar, Iridium NEXT, among others) [1]. These satellites will shower the Earth with a plethora of signals, diverse in frequency and direction, which could be utilized for PNT in a dedicated fashion [2] or opportunistically [3].

To compensate for the limitations of global navigation satellite systems (GNSS) [4], [5], researchers over the past decade studied the exploitation of terrestrial signals of opportunity (SOPs) for PNT. SOPs include: (i) AM/FM radio [6]; (ii) digital television [7]; (iii) WiFi [8]; and (iv) cellular 3G [9], [10], 4G [11], [12], and 5G [13], [14]; with cellular SOPs showing the most promise, as they achieved lane-level positioning on ground vehicles [15], [16], meter-level positioning on high-altitude aircraft [17], and submeter-level positioning on low-altitude unmanned aerial vehicles [18], [19], and are usable in environments under intentional GPS jamming [20]. Exploiting SOPs did not stay earthly, as LEO satellites have received considerable attention recently as potential SOPs [21]. Many theoretical and experimental studies have been conducted on LEO-based PNT [22]–[27].

LEO satellites possess desirable attributes for PNT [2], [3]: (i) they are around twenty times closer to the Earth compared to GNSS satellites, which reside in medium Earth orbit (MEO), which could yield significantly higher carrier-to-noise ratio; (ii) they are becoming abundant as tens thousands of broadband Internet satellites are expected to be deployed into LEO; and (iii) they transmit in different frequency bands and are placed in varying orbits, making LEO satellite signals diverse in frequency and direction. However, exploiting broadband LEO satellite signals for PNT purposes comes with challenges [28], as they are owned by private operators that typically do not disclose crucial information about the satellites': (i) ephemerides, (ii) clock synchronization and stability, and (iii) signal specifications.

To address the first challenge, several approaches have been recently proposed, including differential navigation utilizing a known base receiver [29], [30], simultaneous tracking and navigation (STAN) [31], and analytical/machine-learning satellite

This work was supported in part by the Office of Naval Research (ONR) under Grants N00014-19-1-2511 and N00014-22-1-2242, in part by the Air Force Office of Scientific Research (AFOSR) under Grant FA9550-22-1-0476, and in part by the U.S. Department of Transportation (USDOT) under Grant 69A3552047138 for the CARMEN University Transportation Center (UTC).

orbit tracking [32], [33]. Approaches to address the second challenge have been offered in [24], [34]. To address the third challenge, the paradigm of cognitive opportunistic navigation, which estimates the minimally known LEO satellite signals in a *blind* fashion has been showing tremendous promise [35]. Most recently, this paradigm allowed for the exploitation of unknown Starlink LEO satellites, from which navigation observables were produced via (i) a carrier phase tracking approach [27] and (ii) a generalized likelihood ratio (GLR) Doppler detection approach [36], with the former localizing a receiver to within a two-dimensional (2D) error of 25.9 m, while the latter achieving a 2D error of 10 m.

This paper addresses the third challenge by developing a blind beacon estimation and Doppler tracking framework that is agnostic to the modulation and multiple access scheme adopted by LEO satellites. The proposed framework generates navigation observables from broadband LEO satellites without the need to know their signal specifications. Previous researchers have proposed frameworks for blind estimation of spreading sequences in direct sequence spread spectrum in communication systems [37] and for GPS signals under non-cooperative conditions [38]. However, these approaches cannot be applied to LEO because they do not account for the high dynamics channel between the LEO satellite and a terrestrial receiver. Previous literature has proposed methods for Doppler tracking with M-ary phase shift keying (M-PSK) and orthogonal frequency division multiplexing (OFDM) signals [39]–[41]. The aforementioned approaches aim to generate a peak in the frequency-domain by either relying on nonlinear operations (for M-PSK signals) or increasing the coherent processing interval (CPI) (for OFDM signals). After generating the peak, the methods track it using a peak tracking algorithm to estimate the Doppler shift. However, using nonlinear operations could degrade the signal-to-noise ratio (SNR), while increasing the CPI is not straightforward with the highly dynamic channels encountered with LEO satellites. Also, peak tracking is prone to generate invalid observables and even divergence whenever the spectrum is contaminated by noisy DC peaks.

This paper proposes a novel spectral-based framework to mitigate the above challenges. The proposed framework relies on the presence of a repetitive sequence (also known as a beacon) in the signal transmitted by the LEO satellite that will induce a prominent feature in the received spectrum. The proposed blind Doppler tracker locks on the satellite's feature in the frequency domain and uses the cross-correlation method to track the Doppler shift.While spectral cross-correlation has been studied in the literature [42] and used for noise reduction in speech [43] and detection of stars and planets [44], to the author's knowledge, this approach is newly applied to track Doppler from LEO satellites.

This paper makes the following contributions: (i) develop an analytical approximation of the received signal frequency spectrum under high dynamics channel, (ii) propose a novel blind Doppler estimator using spectral cross-correlation and a Kalman filter (KF)-based tracking loop, (iii) demonstrate successful acquisition, tracking, and positioning with multi-constellation LEO satellite, namely Orbcomm, Iridium NEXT, Starlink, and OneWeb. To the author's knowledge, this paper is the first to show tracking and navigation solution results with the OneWeb LEO constellation. It is important to note that the main purpose of this blind navigation beacon estimation framework is to estimate the time-domain waveform of the repetitive sequence present in the LEO signals. Decoding the repetitive sequence using its modulation scheme is an extra step presented in this paper for the sake of presentation; however, the refined time-domain waveform alone is sufficient to be used to generate navigation observables from LEO satellites. The highlight of the proposed framework is its ability of estimating the transmitted beacon on-the-fly even if the signal structure employed at the satellite's end changes.

In light of recent partnerships by broadband LEO satellite operators and terrestrial cellular providers, it is expected that broadband LEO satellite constellations will move to adopting the 5G new radio (NR) (and generally, the third generation partnership project (3GPP)) standards for cellular communications. In preparation for this, simulation results are presented showing successful beacon estimation and Doppler tracking of Starlink LEO satellites transmitting 5G-NR OFDM signals. Experimental results are also presented demonstrating the efficacy of the proposed framework on multi-constellation LEO satellites, namely OneWeb, Starlink, Orbcomm, and Iridium NEXT. Despite adopting different modulation and multiple access transmission schemes, the proposed framework is capable of successfully estimating the beacon and tracking the Doppler, in a blind fashion, of 8 LEO satellites (2 OneWeb, 4 Starlink, 1 Iridium NEXT, and 1 Orbcomm) over a period of about 560 seconds with Hz-level accuracy. The produced Doppler measurements were fused through a nonlinear least-squares estimator to localize a stationary receiver to an unprecedented level of accuracy. Starting with an initial estimate about 3,600 km away, a final three-dimensional (3–D) position error of 5.8 m and 2–D position error of 5.1 m was achieved. Aside from achieving this unprecedented accuracy, these results represent the first successful opportunistic tracking of unknown OneWeb LEO signals and their exploitation for positioning.

The paper is organized as follows. Section II derives the signal model. Section III introduces the blind Doppler tracking. Section IV develops the code phase tracking. Section V presents the blind beacon estimation. Section VI presents simulation results. Section VIII presents experimental results. Section VIII presents the positioning framework and solution. Section IX gives concluding remarks.

II. Signal Model

This section presents a model of the received signal which takes into account the high dynamics channel between the LEO satellite and ground-based receiver. Then, it derives an analytical expression of the signal's frequency spectrum.

A. Existence of Repetitive Sequences

The proposed framework relies on the existence of a repetitive sequence in the signal transmitted by the LEO satellite. The existence of repetitive sequences in any communication system is not a strong assumption as they are either inherently defined by the source and channel encoding, modulation, and multiplexing schemes, or abundantly transmitted by the communication source for synchronization purposes at the UE. For example, code division multiple access (CDMA) in cellular 3G [45], GPS [46], and Globalstar LEO [47], employ repetitive sequences in the form of pseudorandom noise (PRN) codes to spread the data before transmission. In OFDM used in 4G long-term evolution (LTE) [48] and 5G [49], the primary synchronization sequence (PSS) and secondary synchronization sequence (SSS) define repetitive sequences in the signal transmitted by cellular towers. Moreover, permanently or temporarily repeated patterns in the transmitted user data can define a repetitive sequence. As an example, Orbcomm LEO satellites transmit their ephemeris packets every 4 seconds [50]. The ephemeris packet contains the current date and time, which is temporarily repetitive (the same) along the symbols corresponding to the day, month, and year.

B. Baseband Received Signal Model

Let $x(t)$ be the unknown signal transmitted by a LEO satellite before carrier modulation. The proposed framework does not assume knowledge of any particular modulation or multiplexing scheme. The only assumption is that the transmitted signal $x(t)$ can be written as $x(t) = s(t) + n_d(t)$, where $s(t)$ is a deterministic repetitive signal, and $n_d(t)$ is a random signal driven by the user data. The proposed framework assumes the following properties of $s(t)$:

1) It is periodic with period T_0.
2) It is uncorrelated with the user data $n_d(t)$.
3) It is zero-mean and has a stationary power spectral density (PSD) $\left|\mathcal{F}\left\{s(t)w_{T_0}(t)\right\}\right|^2 = S_s(f)$, where $w_{T_0}(t)$ is a windowing function that is unity within the interval $[0, T_0)$ and zero elsewhere.

Consider $x(t)$ being transmitted at a carrier frequency f_c. Let $\tau_d(t)$ denote the apparent delay between the transmitted signal $x_c(t) \triangleq x(t)\exp(j2\pi f_c t)$ and the received signal at the receiver's antenna. The apparent delay $\tau_d(t)$ is the composition of multiple effects: (i) the time-of-flight along the line-of-sight (LOS) between the transmitter and receiver (i.e., $d_{LOS}(t)/c$, where $d_{LOS}(t)$ is the LOS distance between the LEO satellite's transmitter and the receiver and c is the speed of light); (ii) combined effect of the transmitter's and receiver's clock biases, denoted $\delta t_{clk}(t)$; (iii) ionospheric and tropospheric delays $\delta t_{iono}(t)$ and $\delta t_{tropo}(t)$, respectively; and (iv) other unmodeled errors. After propagating in an additive white Gaussian channel, the resulting received signal before baseband mixing can be expressed as

$$\begin{aligned} r_c(t) &= x_c\left(t - \tau_d(t)\right) + n_c(t) \\ &= x(t - \tau_d(t)) \exp\left[\, j2\pi f_c \left[t - \tau_d\left(t\right)\right]\right] + n_c(t), \end{aligned}$$

where $n_c(t)$ is complex, zero-mean, white Gaussian noise with two-sided PSD $N_0/2$. Let $r^-(t)$ denote the received signal after baseband mixing and filtering, which can be expressed as

$$\begin{aligned} r^-(t) &\triangleq r_c(t)\exp\left(-j2\pi f_c t\right) \\ &= x(t - \tau_d(t))\exp\left[\, j\theta(t)\right] + n^-(t), \end{aligned}$$

where $n^-(t)$ is the low-pass filtered version of $n_c(t)$, and $\theta(t)$ is the carrier phase of the received signal expressed as

$$\theta(t) \triangleq -2\pi f_c \tau_d(t). \tag{1}$$

Using a Taylor series expansion (TSE), at time instant $t_k = t_0 + kT_0$, where k is the sub-accumulation index and t_0 is some initial time; the carrier phase of the received signal $\theta_k(t) \triangleq \theta(t)w_{T_0}(t - t_k)$ for $t \in [0, T_0)$ can be approximated as

$$\theta_k(t) \approx \theta(t_k) + \dot{\theta}(t_k)(t - t_k) + \frac{1}{2}\ddot{\theta}(t_k)(t - t_k)^2. \tag{2}$$

By definition, $f_D(t) \triangleq \frac{\dot{\theta}(t)}{2\pi}$ is the apparent Doppler shift and $\dot{f}_D(t) \triangleq \frac{\ddot{\theta}(t)}{2\pi}$ is the apparent Doppler rate. It is important to note that the channel between the LEO satellite and the opportunistic receiver is highly dynamic, thus, high Doppler shift and rate will be observed by the receiver. On the other, at the k-th sub-accumulation, $\tau_d(t)$ is approximated by its zero-order TSE term $d_k \approx \tau_d(t_k)$ and the higher-order terms are dropped to simplify the following signal analysis. It worth noting that the higher-order terms in the code phase account for compression and dilation of the code in the time-domain, but this paper ignores this effect. The experimental results presented in Section VIII show that such effect is indeed negligible for the Orbcomm, Iridium NEXT, Starlink, and OneWeb LEO constellations. Finally, the expression of the received signal before carrier wipe-off at the k-th sub-accumulation can be expressed as

$$\begin{aligned} r_k^-(t) &\triangleq r^-(t)w_{T_0}(t - t_k) \\ &= s_k(t)\exp\left[\, j\theta_k(t)\right] + n_k^-(t), \end{aligned} \tag{3}$$

where $s_k(t) \triangleq s(t - d_k)w_{T_0}(t)$ and the term $n_k^-(t) \triangleq \left[n^-(t - d_k) + n_d(t - d_k)\right] w_{T_0}(t)$ represents the lumped user data and channel noise. The received signal $r_k(t)$ after carrier wipe-off using the carrier phase estimate, denoted $\hat{\theta}_k(t)$, generated by the tracking loop discussed in Section III-B, can be expressed as

$$\begin{aligned} r_k(t) &= r_k^-(t)\exp\left[\, -j\hat{\theta}_k(t)\right] \\ &= s_k(t)\exp\left[\, j\tilde{\theta}_k(t)\right] + n_k(t), \end{aligned} \tag{4}$$

where $\tilde{\theta}_k(t) = \theta_k(t) - \hat{\theta}_k(t)$ is the residual carrier phase.

C. Frequency Spectrum of the Received Signal

This section derives an analytical expression of the received signal's frequency spectrum at the k-th sub-accumulation, i.e., $S_{r_k}(f) = \left|\mathcal{F}\left\{r_k(t)\right\}\right|^2$. Using the third property of $s(t)$, the

Wigner distribution function (WDF) of $s_k(t)$ for $t \in [0, T_0)$ can be written as

$$W_s(t,f) \triangleq \int_{-\infty}^{\infty} s_k\left(t+\frac{\tau}{2}\right) s_k^*\left(t-\frac{\tau}{2}\right) \exp(-2\pi f\tau)\, d\tau = \frac{S_s(f)}{T_0},$$

where s^* denotes the complex conjugate of s. It can be shown that the WDF of the residual carrier phase at the k-th sub-accumulation $C_k(t) = \exp(j\tilde{\theta}_k(t))$, for $t \in [0, T_0)$, is

$$W_{C_k}(t,f) = \delta\left(f - \frac{\dot{\tilde{\theta}}_k}{2\pi} - \frac{\ddot{\tilde{\theta}}_k}{2\pi} t\right),$$

where $\delta(\cdot)$ is the Dirac delta function. Using the second property of $s(t)$, WDF of $r_k(t)$ in (4), for $t \in [0, T_0)$, becomes

$$W_{r_k}(t,f) = \frac{S_s(f)}{T_0} \circledast \delta\left(f - \frac{\dot{\tilde{\theta}}_k}{2\pi} - \frac{\ddot{\tilde{\theta}}_k}{2\pi} t\right) + W_{n_k}(t,f),$$

where $(f \circledast g)(t) = \int_{-\infty}^{\infty} f(\tau) g(t-\tau) d\tau$ is the convolution of f and g and $W_{n_k}(t,f)$ is the WDF of the noise and data at the k-th sub-accumulation.

Using the projection property of WDF, the frequency spectrum $S_{r_k}(f) \triangleq \int_0^{T_0} W_{r_k}(t,f)\, dt$ can be further expressed as

$$\begin{aligned} S_{r_k}(f) &= \frac{S_s(f)}{T_0} \circledast \int_0^{T_0} \delta\left(f - \frac{\dot{\tilde{\theta}}_k}{2\pi} - \frac{\ddot{\tilde{\theta}}_k}{2\pi} t\right) dt + S_{n_k}(f) \\ &= S_s(f) \circledast \frac{2\pi}{\left|\ddot{\tilde{\theta}}_k\right| T_0} \int_0^{T_0} \delta\left(t - \frac{2\pi f - \dot{\tilde{\theta}}_k}{\ddot{\tilde{\theta}}_k}\right) dt + S_{n_k}(f) \\ &= S_s(f) \circledast \Pi\left(f; \dot{\tilde{\theta}}_k, \ddot{\tilde{\theta}}_k\right) + S_{n_k}(f), \end{aligned} \tag{5}$$

where $S_{n_k}(f) = \int_0^{T_0} W_{n_k}(t,f)\, dt$ and

$$\Pi\left(f; \dot{\theta}, \ddot{\theta}\right) \triangleq \frac{2\pi}{\left|\ddot{\theta}\right| T_0} \begin{cases} 1, & \left| f - \dfrac{\dot{\theta} + \frac{|\ddot{\theta}|}{2} T_0}{2\pi} \right| < \dfrac{|\ddot{\theta}|}{4\pi} T_0 \\ 0, & \text{elsewhere} \end{cases}.$$

Equation (5) implies that the received signal's frequency spectrum consists of a shifted and dilated version of the repetitive sequence's frequency spectrum alongside noise. The shift in the received spectrum is due to the residual Doppler $\dot{\tilde{\theta}}_k$, while the dilation is due to the residual Doppler rate $\ddot{\theta}_k$.

III. Blind Doppler Tracking

This section derives the Doppler discriminator and formulates the KF-based Doppler tracking loop.

A. Frequency Domain-Based Doppler Discriminator

The nonlinear least-squares (NLS) estimator of the residual Doppler $\dot{\tilde{\theta}}_k$ at the k-th sub-accumulation is given by

$$\dot{\tilde{\theta}}_k = \underset{\dot{\theta}}{\operatorname{argmin}} \left\| S_{r_k}(f) - S_s(f) \circledast \Pi\left(f; \dot{\theta}, \ddot{\theta}\right) \right\|^2 \tag{6}$$

$$\begin{aligned} \dot{\tilde{\theta}}_k &= \underset{\dot{\theta}}{\operatorname{argmin}} \|S_{r_k}(f)\|^2 + \left\| S_s(f) \circledast \Pi\left(f; \dot{\theta}, \ddot{\theta}\right) \right\|^2 \\ &\quad -2 \left(S_{r_k} \star S_s\right)(f) \circledast \Pi\left(f; \dot{\theta}, \ddot{\theta}\right) \qquad (7) \\ &= \underset{\dot{\theta}}{\operatorname{argmax}} \left(S_{r_k} \star S_s\right)(f) \circledast \Pi\left(f; \dot{\theta}, \ddot{\theta}\right) \\ &\approx \underset{\dot{\theta}}{\operatorname{argmax}} \left(S_{r_k} \star S_s\right)(f) \circledast \delta\left(f - \frac{\dot{\theta}}{2\pi}\right), \quad \text{for} \quad \ddot{\tilde{\theta}}_k \approx 0 \\ &= 2\pi \underset{f}{\operatorname{argmax}} \left(S_{r_k} \star S_s\right)(f), \qquad (8) \end{aligned}$$

where $(f \star g)(\tau) = \int_{-\infty}^{\infty} f^*(t) g(t+\tau) dt$ is the cross-correlation of f and g. The first two terms in the minimization problem in (7) are a constant function of the optimization parameter $\dot{\theta}$; therefore, they are ignored. Since the blind receiver does not have prior knowledge of $S_s(f)$, it starts with an initial estimate $\hat{S}_s(f) \equiv S_{r_0}(f)$ and refines the repetitive sequence's spectrum with every sub-accumulation. This initialization approach introduces a Doppler ambiguity $\dot{\tilde{\theta}}_0$ invoked by taking $S_{r_0}(f)$ as initial spectral reference for Doppler tracking. Nonetheless, this Doppler ambiguity can be resolved as will be discussed in the Section V-C. Note that the assumption $\ddot{\tilde{\theta}}_k \approx 0$ (i.e., regime of small residual Doppler rate values) invoked in (8) is a reasonable assumption, since the Doppler rate between two consecutive sub-accumulations is nearly constant for LEO satellite channels.

B. KF-Based Tracking Loop

The continuous-time signal in (4) is sampled at a constant sampling interval $T_s = 1/F_s$. The discrete-time received signal before carrier wipe-off at the k-th sub-accumulation can be written as

$$r_k^-[n] = s[n - d_k] \exp\left(j\Theta_k[n]\right) + n_k^-[n], \tag{9}$$

where $n \in [0, L-1]$; $s[n]$ is the discrete-time equivalent of $s(t)$ with period $L = T_0/T_s$; $\Theta_k[n]$ and d_k are the discrete-time carrier phase and code phase, respectively, of the received signal at the k-th sub-accumulation; and $n_k^-[n]$ is the discrete-time equivalent of $n_k^-(t)$.

The continuous-time carrier phase state vector is defined as $\boldsymbol{\theta}(t) \triangleq \left[\theta(t),\ \dot{\theta}(t),\ \ddot{\theta}(t)\right]^{\mathsf{T}}$, with dynamics modeled as

$$\dot{\boldsymbol{\theta}}(t) = \mathbf{A}\boldsymbol{\theta}(t) + \mathbf{B}\boldsymbol{w}(t), \tag{10}$$

$$\mathbf{A} \triangleq \begin{bmatrix} 0 & 1 & 0 \\ 0 & 0 & 1 \\ 0 & 0 & 0 \end{bmatrix}, \quad \mathbf{B} \triangleq \begin{bmatrix} 0 \\ 0 \\ 1 \end{bmatrix},$$

where $\boldsymbol{w}(t)$ is a zero-mean white noise process with PSD q_w. The continuous-time model (10) is discretized at a constant sampling time $T_0 = LT_s$ leading to

$$\boldsymbol{\Theta}_{k+1} = \mathbf{F}\boldsymbol{\Theta}_k + \mathbf{w}_k, \tag{11}$$

where $\boldsymbol{\Theta}_k \triangleq \left[\theta_k,\ \dot{\theta}_k,\ \ddot{\theta}_k\right]^{\mathsf{T}}$ is the carrier phase state at the k-th sub-accumulation, $\mathbf{F} \triangleq e^{\mathbf{A}T_0}$ is the state transition matrix, and $\mathbf{w}_k$ is a discrete-time process noise, which is

a zero-mean white random sequence with covariance $\mathbf{Q} = q_w \int_0^{T_0} e^{\mathbf{A}t}\mathbf{B}\big(e^{\mathbf{A}t}\mathbf{B}\big)^{\mathsf{T}} dt$. The reconstructed sequence of the carrier phase that is used to perform carrier wipe-off can be written as a second-order piecewise polynomial given by $\hat{\Theta}_k[n] = \hat{\theta}_{k-1} + \hat{\dot{\theta}}_k n T_s + \frac{1}{2}\hat{\ddot{\theta}}_k (nT_s)^2$, $n \in [0, L-1]$. After carrier wipe-off, the received signal's sequence becomes

$$\begin{aligned} r_k[n] &= r_k^-[n] \exp\left[-j\hat{\Theta}_k[n]\right] \\ &= s\left[n - d_k\right] \exp\left[j\tilde{\Theta}_k[n]\right] + n_k[n]. \end{aligned} \tag{12}$$

Equation (12) will be used to determine the residual Doppler $\tilde{\dot{\theta}}_k$ at the k-th sub-accumulation, which is fed as innovation to a KF loop that uses the observation model

$$z_k = \mathbf{C}\boldsymbol{\Theta}_k + v_k, \quad \mathbf{C} \triangleq \begin{bmatrix} 0 & 1 & 0 \end{bmatrix}, \tag{13}$$

where v_k is a discrete-time zero-mean white noise sequence with variance σ_{θ}^2. The proposed KF innovation ν_k is the fast Fourier transform (FFT)-based discrete version of (8).

$$\nu_{\text{KF}}(k) = \tilde{\dot{\theta}}_k = 2\pi \operatorname*{argmax}_f |R_k[f]|^2 \star \left|\hat{S}_k[f]\right|^2,$$

where $R_k[f]$ and $\hat{S}_k[f]$ are the FFT of $r_k[n]$ and $s[n]$, respectively. The proposed blind Doppler tracking loop can be considered to be in the locked regime whenever the innovation sequence ν_k becomes nearly white and its variance stabilizes. In this regime, $\tilde{\boldsymbol{\Theta}}_k \approx [0, 0, 0]^{\mathsf{T}}$ and $r_k[n] \approx s\left[n - d_k\right] + n_k[n]$.

Note that the KF is initialized with $\hat{\boldsymbol{\Theta}}_0 \equiv \left[\hat{\theta}_0,\, \hat{\dot{\theta}}_0,\, \hat{\ddot{\theta}}_0\right]^{\mathsf{T}}$ that gives rise to an initial carrier phase state error $\tilde{\boldsymbol{\Theta}}_0 \equiv \left[\tilde{\theta}_0,\, \tilde{\dot{\theta}}_0,\, \tilde{\ddot{\theta}}_0\right]^{\mathsf{T}}$. It can be readily shown that for the observation matrix $\mathbf{C}$ defined in (13), the initial carrier phase error $\tilde{\theta}_0$ is unobservable. This will induce a shift in the phase of the estimated repetitive sequence, causing the initial Doppler error $\tilde{\dot{\theta}}_0$ to persist as an ambiguity in the tracked Doppler $\hat{\dot{\theta}}_k$ (since it is embedded into the first received sub-accumulation which is taken as reference for tracking). Due to the linearity and time-invariance of (11) and (13), it can be readily shown that the residual carrier phase state vector $\tilde{\boldsymbol{\Theta}}_k$ will converge to zero. Fig. 1 summarizes the proposed blind Doppler tracking.

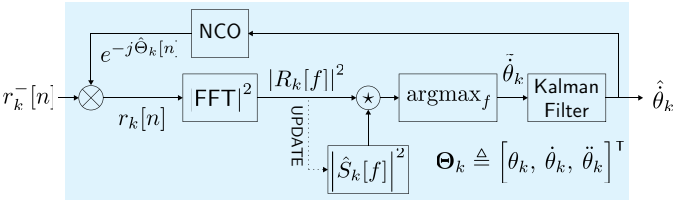

Fig. 1. Block diagram of the proposed blind Doppler tracking loop. NCO: numerically controlled oscillator.

IV. Code Phase Tracking

After the blind Doppler tracking loop achieves lock, the blind receiver starts to correct the carrier phase changes and tracks the code phase of the repetitive sequence. Given (12), the NLS estimate of the code phase at the k-th sub-accumulation is given by

$$\begin{aligned} \hat{d}_k &= \operatorname*{argmin}_d \|r_k[n] - s[n-d]\|^2 \\ &= \operatorname*{argmin}_d \left\{\|r_k[n]\|^2 + \|s[n-d]\|^2 - 2(r_k \star s)[d]\right\} \\ &= \operatorname*{argmax}_d (r_k \star s)[d]. \end{aligned} \tag{14}$$

It is important to note that the NLS code phase estimator given by (14) is only valid while the Doppler tracking loop is locked and the carrier phase changes are tracked and wiped-off at every sub-accumulation. Without the lock condition, the residual carrier phase sequence $\tilde{\Theta}_k[n]$ present in (12) deteriorates the NLS estimator performance drastically. Furthermore, as the blind receiver does not have prior knowledge of $s[n]$, it starts with an initial estimate $\hat{s}[n] \equiv r_0[n]$ and uses it as a reference to track the code phase $\hat{d}_k$. This initialization approach introduces a code phase ambiguity d_0. After tracking the code phase $\hat{d}_k$, the receiver corrects for this code phase shift as follows

$$\begin{aligned} \bar{r}_k[n] &\triangleq r_k[n] \otimes \hat{d}_k \\ &= s\left[n - \tilde{d}_k\right] \exp\left[j\tilde{\Theta}_k[n]\right] + n_k[n], \end{aligned} \tag{15}$$

where $(x[n] \otimes d)$ denotes the circular shift operation that shifts the sequence $x[n]$ by d samples, and $\tilde{d}_k = d_k - \hat{d}_k$ is the code phase error at the k-th sub-accumulation.

V. Blind Navigation Beacon Estimation

This section discusses the blind navigation beacon estimation framework. Given (9), the time-varying parameters modulating the deterministic repetitive beacon sequence $s[n]$ are: (i) the carrier phase state vector $\boldsymbol{\Theta}_k$ and (ii) the code phase d_k. Sections III and IV discussed the mechanism of tracking and wiping-off the effect of these time-varying parameters. In the regime of successful Doppler and code phase tracking $\left\{\tilde{\Theta}_k[n] \approx 0,\ \tilde{d}_k \approx 0\right\}$, (15) simplifies to $\bar{r}_k[n] \approx s[n] + n_k[n]$. At this stage, the receiver is ready to (i) blindly estimate the deterministic repetitive sequence present in (15) and (ii) resolve for the Doppler ambiguity associated with the estimated repetitive sequence.

A. Beacon Estimator Formulation

Let $\boldsymbol{r}_k$, $\boldsymbol{n}_k$, $\boldsymbol{s}$, $\boldsymbol{y}$, $\mathbf{H}$, and $\boldsymbol{w}$ denote the equivalent complex vector form of the terms in (15) such that

$$\begin{aligned} \boldsymbol{r}_k &\triangleq \begin{bmatrix} \bar{r}_k[0], & \ldots, & \bar{r}_k[L-1] \end{bmatrix}^{\mathsf{T}}, \\ \boldsymbol{n}_k &\triangleq \begin{bmatrix} n_k[0], & \ldots, & n_k[L-1] \end{bmatrix}^{\mathsf{T}}, \\ \boldsymbol{s} &\triangleq \begin{bmatrix} s[0], & \ldots, & s[L-1] \end{bmatrix}^{\mathsf{T}}, \\ \boldsymbol{y} &\triangleq \begin{bmatrix} \boldsymbol{r}_1^{\mathsf{T}}, & \ldots, & \boldsymbol{r}_M^{\mathsf{T}} \end{bmatrix}^{\mathsf{T}}, \\ \boldsymbol{w} &\triangleq \begin{bmatrix} \boldsymbol{n}_1^{\mathsf{T}}, & \ldots, & \boldsymbol{n}_M^{\mathsf{T}} \end{bmatrix}^{\mathsf{T}}, \\ \mathbf{H} &\triangleq \begin{bmatrix} \mathbf{I}_L, & \ldots, & \mathbf{I}_L \end{bmatrix}^{\mathsf{T}}, \end{aligned}$$

where $\mathbf{I}_L$ denotes the identity matrix of size $L \times L$; $\boldsymbol{r}_k$ and $\boldsymbol{n}_k$ denote the vectors of observed and noise samples

at the k-th sub-accumulation, respectively; $\boldsymbol{y}$ and $\boldsymbol{w}$ denote the vectors of concatenated observations and noise of M sub-accumulations, respectively; $\boldsymbol{s}$ denotes the vector of the deterministic repetitive sequence present in the received signal that is sought to be estimated; and $\mathbf{H}$ denotes the observation matrix of the M sub-accumulations in the regime of Doppler and code phase tracking lock. One can readily write the vector of observed samples as

$$\boldsymbol{y} = \mathbf{H}\boldsymbol{s} + \boldsymbol{w}, \tag{16}$$

where $\boldsymbol{w}$ is as zero-mean white noise sequence with covariance $\mathbf{R} = \sigma_n^2 \mathbf{I}_{L\times M}$. Given the observation model in (16), the least-squares estimate of the repetitive sequence $\boldsymbol{s}$ is given by

$$\hat{\boldsymbol{s}}_M = \left(\mathbf{H}^{\mathsf{H}}\mathbf{H}\right)^{-1}\mathbf{H}^{\mathsf{H}}\boldsymbol{y} = \frac{1}{M}\sum_{k=1}^{M}\boldsymbol{r}_k, \tag{17}$$

where $(.)^{\mathsf{H}}$ denotes the Hermitian transpose operator.

B. Convergence Property

This section studies the convergence property and stopping criterion for the beacon estimator given in (17). The energy in the estimated sequence, $\hat{\boldsymbol{s}}_M$, after M sub-accumulations can be expressed as

$$\begin{aligned}\mathbb{E}\left\{\|\hat{\boldsymbol{s}}_M\|^2\right\} &= \mathbb{E}\left\{\frac{1}{M^2}\sum_{j=1}^{M}\sum_{k=1}^{M}\boldsymbol{r}_j{}^{\mathsf{H}}\boldsymbol{r}_k\right\}\\ &= \|\boldsymbol{s}\|^2 + \frac{2}{M}\sum_{k=1}^{M}\mathbb{E}\left\{\boldsymbol{s}^{\mathsf{H}}\boldsymbol{n}_k\right\} + \frac{1}{M^2}\sum_{j=1}^{M}\sum_{k=1}^{M}\mathbb{E}\left\{\boldsymbol{n}_j{}^{\mathsf{H}}\boldsymbol{n}_k\right\}\\ &= \|\boldsymbol{s}\|^2 + \frac{L\sigma_n^2}{M}.\end{aligned} \tag{18}$$

The fact that $\mathbb{E}\left\{\boldsymbol{s}^{\mathsf{H}}\boldsymbol{n}_k\right\} = 0$ follows from the second and third properties of $s(t)$, while $\mathbb{E}\left\{\boldsymbol{n}_j{}^{\mathsf{H}}\boldsymbol{n}_k\right\} = L\sigma_n^2\delta_{ij}$, where δ_{ij} is the Kronecker delta function, follows from the assumed whiteness of the noise. According to (18), $\lim_{M\to\infty}\mathbb{E}\left\{\|\hat{\boldsymbol{s}}_M\|^2\right\} = \|\boldsymbol{s}\|^2$; therefore, the energy in the estimated beacon decreases with every additional observed sub-accumulation until reaching a steady-state value equal to the energy of the true beacon $\|\boldsymbol{s}\|^2$. This gives a recipe for a stopping criterion for the beacon estimator given as

$$\frac{\|\hat{\boldsymbol{s}}_M\|^2}{\|\hat{\boldsymbol{s}}_{M-1}\|^2} \geq \eta_{th},$$

where η_{th} is a predetermined constant chosen to be 0.9 for the purposes of this paper.

C. Doppler Ambiguity Resolution

To resolve the Doppler ambiguity $\tilde{\dot{\theta}}_0$ present in the estimated repetitive sequence, the receiver relies on the relationship between the carrier and code phase tracking loops discussed in Section III and Section IV, respectively. Let $\dot{\theta}_k = \hat{\dot{\theta}}_k - \tilde{\dot{\theta}}_0 + \nu_{\dot{\theta},k}$ denotes the true ambiguity-free Doppler shift, where $\nu_{\dot{\theta},k}$ is a discrete-time frequency noise. Therefore, the true carrier phase θ_k can be expressed as

$$\begin{aligned}\theta_k &\triangleq \sum_{j=0}^{k-1}\dot{\theta}_j T_0 + \theta_0 = \sum_{j=0}^{k-1}(\hat{\dot{\theta}}_j - \tilde{\dot{\theta}}_0)T_0 + \nu_{\theta,k}\\ &= \hat{\theta}_k - \tilde{\dot{\theta}}_0 k T_0 + \theta_0 + \nu_{\theta,k},\end{aligned} \tag{19}$$

where θ_0 is the initial carrier phase ambiguity.

Let $d_k = \hat{d}_k + d_0 + \nu_{d,k}$ be the true code phase, where $\nu_{d,k}$ is the discrete-time code phase noise. The discretization of (1) relating the code and carrier phase yields

$$\theta_k = -2\pi f_c d_k = -2\pi f_c(\hat{d}_k + d_0 + \nu_{d,k}). \tag{20}$$

Equating (19) and (20) leads to

$$y_k = \tilde{\dot{\theta}}_0(kT_0) + b_0 + \nu_k, \tag{21}$$

where $y_k = \hat{\theta}_k + 2\pi f_c \hat{d}_k$ denotes the residual carrier phase, which is a function of the ambiguous Doppler term $\tilde{\dot{\theta}}_0$, $b_0 = -(\theta_0 + 2\pi f_c d_0)$ is the lumped ambiguity term, and $\nu_k = (\nu_{\theta,k} - 2\pi f_c \nu_{d,k})$ is the lumped code and carrier phase noise. With enough sub-accumulations M, $\tilde{\dot{\theta}}_0$ can be estimated from (21) by fitting a linear regression model with y_k as the target variable and kT_0 as the regressor.

VI. Simulation Results

This section demonstrates, via numerical simulations, the ability of the proposed framework to blindly estimate the beacon transmitted by a LEO satellite. To this end, following the notation described in (9), the deterministic repetitive sequence $s[n]$ is chosen to be the Synchronization Sequence Block (SSB) of the 5G-NR frame structure with period T_0, bandwidth B, and energy $\|\boldsymbol{s}\|^2$, as described by the 3GPP. The phase $\Theta_k[n]$ was assumed to follow the Doppler profile of a Starlink LEO satellite and the noise component of the signal $n_k^-[n]$ is modeled as a white random process with PSD $L\sigma_n^2$. Table I summarizes all other simulation parameters.

TABLE I
Simulation Parameters of Emulated 5G Signals Transmitted by Starlink LEO Satellites

Parameter	Value	Unit
$\|\boldsymbol{s}\|^2$	0.003	J
B	5	MHz
SNR	0	dB
T_0	20	ms
f_D	[-250 , 250]	kHz
$\dot{f}_D$	[-3 , 0]	kHz

The first step in the process of blindly estimating the beacon is to perform Doppler wipe-off. As described in Section III-A, the proposed framework only relies on the assumption that the PSD of the deterministic repetitive sequence in a received signal is stationary. Therefore, the framework is capable of tracking and wiping off the Doppler with no *a priori* knowledge of the temporal or spectral signal structure. After

successful Doppler wipe-off, the receiver begins the estimation and refinement of the repetitive sequence. Fig. 2 shows the simulation results of the proposed blind framework, which demonstrates its ability to successfully estimate the 5G frame transmitted by a Starlink LEO satellite.

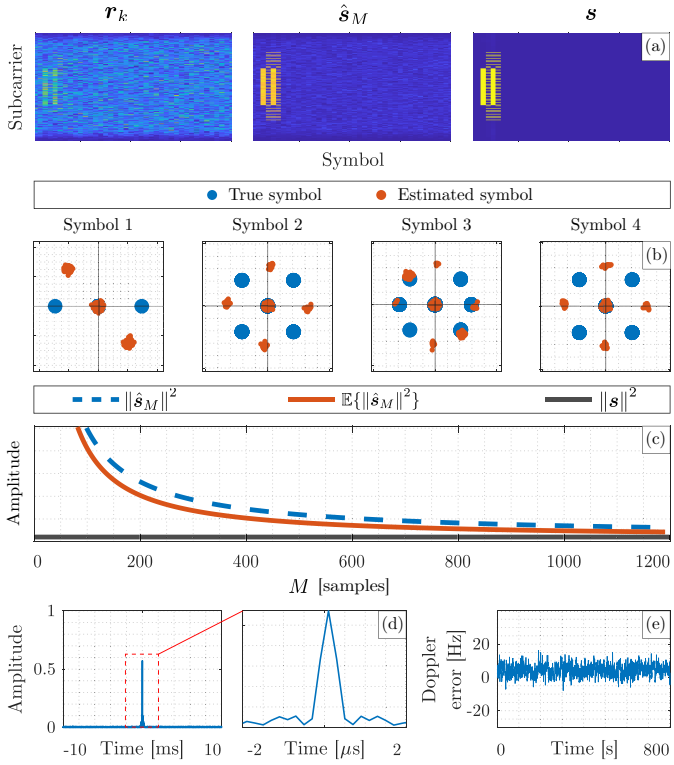

Fig. 2. Simulation results showing successful blind beacon estimation and Doppler tracking of emulated 5G-NR signals transmitted by Starlink LEO satellites: (a) Left: frame of an observed sample sub-accumulation on the left, Middle: refined repetitive sequence after M sub-accumulations, Right: ground truth repetitive sequence's frame. (b) In-phase and quadrature (IQ) components of the estimated sequence and the true sequence. (c) Black: true repetitive sequence's energy. Blue: the energy of the realization shown in (a) and (b). Orange: the expected energy (cf. (18)) of the the estimated sequence $\|\hat{s}_M\|^2$ versus the number of observed sub-accumulations M, respectively. (d) The normalized cross-correlation function between the estimated and true repetitive sequence. (e) The error between the true Doppler shift and the one estimated using the proposed blind Doppler tracker.

In particular, Fig. 2(a) shows the frame of (i) an observed sample sub-accumulation $\boldsymbol{r}_k$ that is composed of the repetitive sequence alongside data and channel noise, (ii) the refined repetitive sequence $\hat{\boldsymbol{s}}_M$ after M sub-accumulations, and (iii) the ground truth repetitive sequence. Fig. 2(b) compares the IQ components of the estimated sequence versus the true sequence. The 5G-NR SSB, which is taken as the repetitive sequence for this simulation, consists of 4 OFDM symbols which are the: (i) PSS at symbol 1, (ii) SSS at symbol 3, and (iii) physical broadcast channel (PBCH) at symbols 2 to 4. Moreover, Fig. 2(b) shows the unobservable constant phase shift $\tilde{\theta}_0$, which is embedded into the estimated sequence relative to the true sequence's constellation. Fig. 2(c) plots in blue the energy of the estimated sequence $\|\hat{\boldsymbol{s}}_M\|^2$ versus the number of observed sub-accumulations M. This curve follows the shape of the theoretical curve $\mathbb{E}\left\{\|\hat{\boldsymbol{s}}_M\|^2\right\}$ discussed in Section V-B, shown in orange. The black curve represent the true repetitive sequence's energy, $\|\boldsymbol{s}\|^2$, which lower-bounds the energy of the estimated sequence. Fig. 2(d) shows the normalized cross-correlation function between the estimated and true repetitive sequence. The prominent cross-correlation peak is an indicator of successful beacon estimation. Finally, Fig. 2(e) shows the error between the true Doppler shift and the one estimated using the proposed blind Doppler tracker during the satellite pass, implying that the proposed framework is capable of tracking the Doppler with Hz-level accuracy– this will also be demonstrated experimentally on the four LEO constellations: Orbcomm, Iridium NEXT, Starlink, and OneWeb in Section VIII-C.

VII. Experimental Results: Beacon Estimation and Blind Doppler Tracking of Orbcomm, Iridium NEXT, Starlink, and OneWeb LEO Constellations

This section presents experimental results demonstrating successful beacon estimation and blind Doppler tracking for four LEO constellations, namely Orbcomm, Iridium NEXT, Starlink, and OneWeb, which transmit their downlink signals according to different modulation schemes. The receiver initializes with and tracks the signal's stationary PSD to generate Doppler observables. Finally, a positioning solution is generated using the estimated observables. Fig. 3 overviews the hardware components used to receive downlink signals from the four LEO constellations. The captured samples were stored and then processed via a software-defined radio implementation (SDR) of the proposed framework.

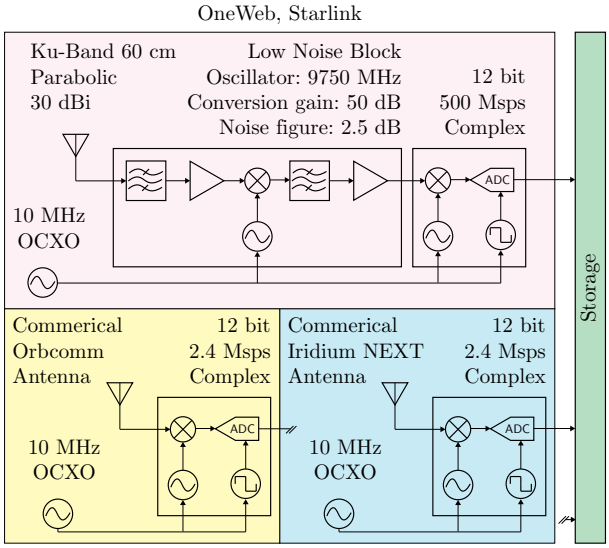

Fig. 3. Block diagram of Orbcomm, Iridium NEXT, Starlink, and OneWeb satellites signal capture setup.

A. Orbcomm LEO Constellation

The proposed blind beacon estimation method was applied to downlink Orbcomm LEO satellite signals. To this end, a stationary National Instrument (NI) universal software radio peripheral (USRP) E312 was equipped with a commercial

Orbcomm antenna to receive signals in the VHF–band. The sampling bandwidth F_s was set to 2.4 MHz and the carrier frequency f_c was set to 137 MHz. The duration of the recorded data was 900 seconds. Orbcomm satellites transmit at a predefined set of frequency pairs in the user downlink spectrum with an effective channel bandwidth $B = 4.8$ kHz. After collection, the Orbcomm signal was fed to the proposed blind beacon estimator and Doppler tracker. On the other hand, for comparative purposes, the true transmitted data of the Orbcomm satellites was decoded using the scheme described in [51]. After decoding, the signal auto-correlation showed repetitive behavior every T_0 intervals equating to 1 second. The decoded data was averaged in a T_0-window over a sufficient number of sub-accumulations to increase the effective energy of the repetitive sequence. Finally, the blindly estimated beacon was compared against the true sequence obtained by the averaging process. Fig. 4(a) shows the true versus estimated sequences in-phase time-domain waveform. Fig. 4(b) shows the IQ plot of the estimated repetitive sequence; this reveals that the modulation scheme of the repetitive sequence for Orbcomm is 4-PSK . Fig. 4(c) shows the cross-correlation function between the true and estimated sequence. The prominent peak indicates successful estimation of the repetitive sequence. Furthermore,

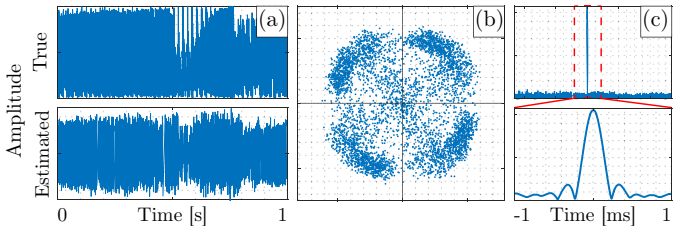

Fig. 4. Blind beacon estimation of Orbcomm LEO satellite signals: (a) In-quadrature waveform of the true versus estimated Orbcomm's repetitive sequence. (b) IQ plot of the estimated repetitive sequence. (c) Cross-correlation function between the true and estimated repetitive sequence. The bottom figure is a zoomed version of the peak in the top figure, which confirms successful beacon estimation.

Fig. 5 shows the result of correlating the estimated repetitive sequence with the collected Orbcomm data. The correlation peaks confirms correct estimation of the repetitive sequence.

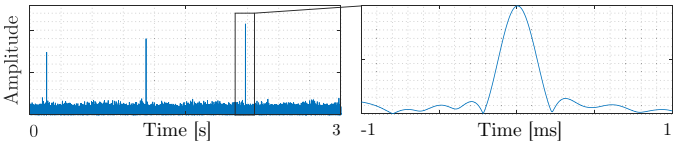

Fig. 5. Correlation of estimated repetitive sequence and Orbcomm data.

B. Iridium NEXT LEO Constellation

An NI-USRP E312 was used to capture raw signal measurements received by a commercial Iridium NEXT antenna. The sampling bandwidth F_s was set to 2.4 MHz, the carrier frequency f_c was set to 1626.2708 MHz in the L–band, which coincide with the ring alert (RA) channel of Iridium satellites, and the total capture duration was 600 seconds. Iridium NEXT satellites employs both time division multiple access (TDMA) and frequency division multiple access (FDMA). The Iridium spectrum consists of multiple channels, namely, the RA, paging channel, voice channel, and duplex user channels. The RA channel bandwidth is $B = 41.667$ kHz and the repetitive sequence period is $T_0 = 90$ ms. Running the blind framework on the collected signal resulted in the repetitive sequence estimate shown in Fig. 6(a). Taking a closer look at the estimated sequence reveals a pure tone sequence (green region) followed by an alternating Binary Phase Shift Keying (BPSK) sequence (red region). This specific estimated repetitive sequence is well-known in the communication literature: it is the typical TDMA synchronization preamble employed in TDMA-based satellite systems [52]. The IQ plot of the estimated repetitive sequence is shown in Fig. 6(b), which indeed matches Figure (1) in [52]. Fig. 6(c) shows the auto-correlation profile of the estimated preamble sequence, which confirms successful sequence estimation. Furthermore, Fig. (7) shows the result of correlating the estimated repetitive sequence with the collected Iridium NEXT data. The correlation peaks separated confirms correct estimation of the repetitive sequence.

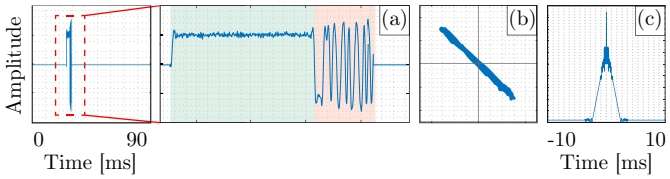

Fig. 6. Blind beacon estimation of Iridium NEXT LEO satellite signals: (a Left: In-phase waveform of the estimated Iridium NEXT's repetitive sequence. Right: zoomed version showing the estimated pure tone sequence (green region) followed by alternating BPSK sequence (red region). (b) IQ plot of the estimated repetitive sequence. (c) Auto-correlation function of the estimated repetitive sequence, which confirms successful beacon estimation.

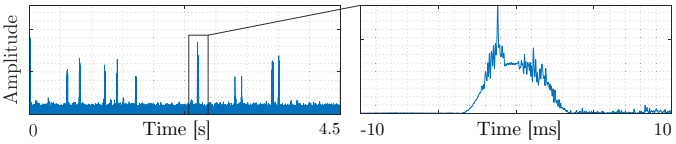

Fig. 7. Correlation of estimated repetitive sequence and Iridium NEXT data.

C. Starlink LEO Constellation

The signal capture setup for Starlink utilized the NI-USRP x410 to collect raw IQ measurements. The sampling bandwidth F_s was set to 500 MHz, the carrier frequency f_c was set to 11.325 GHz, which is roughly at the center of one of Starlink's downlink channels in the Ku–band. According to the Federal Communications Commission (FCC), the Starlink user downlink signal spectrum spans the 10.7 – 12.7 GHz frequency band. This spectrum is dissected into 8 equidistant channels, each with bandwidth $B = 240$ MHz. The period of the repetitive sequence was determined by inspecting the auto-correlation function of a data snapshot that entails many frames. The repetitive sequence present in the frames of the data snapshot induces an impulse train in the auto-correlation function with spacing equal to T_0, which was recorded to

be equal to $4/3$ ms for Starlink downlink signals. A low-noise block (LNB) downconverter was coupled with a 30 dBi conversion gain Ku–band parabolic dish in order to improve the received SNR. The dish was continuously pointed towards the Starlink satellite throughout its passing– propagating the satellite's trajectory from the publicly available TLE files governs the direction in which the dish should be pointed. The NI-USRP x410 was set to record for a duration of 900 seconds. Next, the proposed framework was used to acquire and track the signals present in the collected data. Taking a closer look at the estimated Starlink repetitive sequence reveals an interesting signal structure. Fig. 8(a) shows the auto-correlation profile of the estimated sequence. The different peaks in this figure reveals special values in Starlink's OFDM frame structure, such as the symbol duration, cyclic prefix duration (which is defined as the number of samples taken from the end of a symbol and repeated at its beginning), and the frame duration. Fig. 8(b) shows that the estimated sequence has repetitive components in symbols [1,2,3,5,7]. The parameter estimates from Fig. 8(a) are sufficient to allow for removal of the cyclic prefix from each symbol, which is then followed by applying a short-term Fourier transform (STFT) to the sequence estimate. This allows for spectral analysis of the repetitive sequence which, as shown in Fig. 8(c), reveals 4 silent subcarriers in the middle of the signal bandwidth. In fact, this is the bandwidth location where some tones can be observed sometimes. Fig. 8(d) shows the IQ plot of some of the synchronization sequence bearing symbols. Observing the constellations, it is noted that these synchronization symbols use a 4-quadrature amplitude modulation (QAM) scheme.Note that the first plot (left) is derived from the time domain representation of the symbol whereas the other 2 are derived from the frequency domain representation of the symbols. The estimated repetitive sequences are comparable to the synchronization sequences employed in a 5G-NR (PSS, SSS, and PBCH) frame according to the 3GPP standard.

D. OneWeb LEO Constellation

The signal capture setup for OneWeb downlink signals was the same as that of Starlink with the sampling frequency F_s set to 50 MHz and the carrier frequency f_c set to 11.075 GHz. According to the FCC, OneWeb's user downlink signal spectrum spans the 10.7 – 12.7 GHz frequency band. This spectrum is dissected into 8 equidistant channels, each with bandwidth $B = 250$ MHz. The repetitive sequence period was estimated to be $T_0 = 10$ ms from the data snapshot auto-correlation function. The proposed blind beacon estimation framework was capable of estimating a repetitive sequence which can be used to generate Doppler and code phase observables; these will be shown in the positioning solution presented in Section VIII. To the authors' knowledge, the achieved acquisition and tracking of OneWeb signals is unprecedented in the literature. Fig. (10) shows the result of correlating the estimated repetitive sequence with the collected OneWeb data. The clean correlation peaks separated by T_0 seconds confirms correct estimation of the repetitive sequence. Furthermore, Fig. (9) shows the result of correlating the estimated repetitive sequence with the collected Starlink data. The clean correlation peaks separated by T_0 seconds confirms correct estimation of the repetitive sequence.

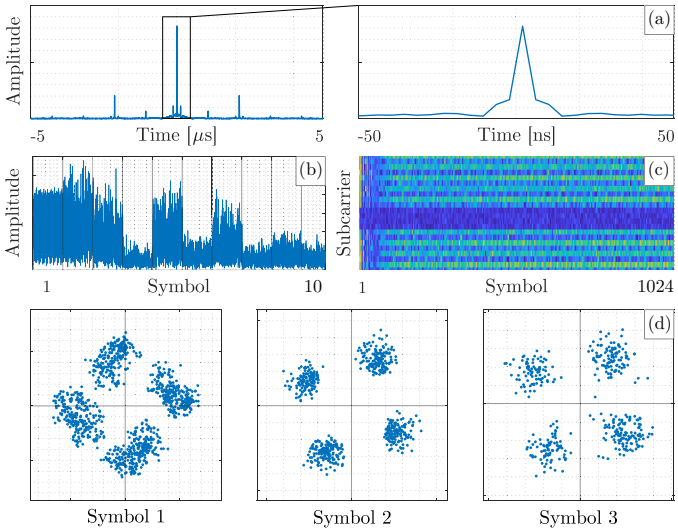

Fig. 8. Blind beacon estimation of Starlink LEO satellite signals: (a) auto-correlation profile of the estimated sequence, (b) frame structure of the estimated time domain repetitive sequence, (c) the OFDM frame structure of the estimated repetitive sequence, and (d) IQ plots of the first three symbols within the sequence.

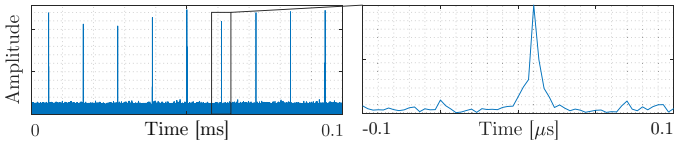

Fig. 9. Correlation of estimated repetitive sequence and Starlink data.

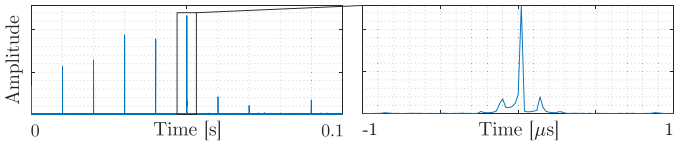

Fig. 10. Correlation of estimated repetitive sequence and OneWeb data.

VIII. Experimental Results: Positioning with Orbcomm, Iridium NEXT, Starlink, and OneWeb LEO Constellations

This section presents the first ever multi-constellation positioning results, exploiting signals from Orbcomm, Iridium NEXT, Starlink, and OneWeb LEO constellations. The carrier phase navigation observables produced by the proposed blind beacon estimation and Doppler tracking framework, for each individual constellation as well as fused from all four constellations, are used to localize a stationary receiver.

A. Carrier Phase Measurement Model

Let $i \in [1, L]$ denote the satellite's index, where L is the total number of satellites. The carrier phase observable $\Phi_i(k) \triangleq \sum_{j=0}^{k-1} c\frac{\hat{\dot{\theta}}_j}{2\pi f_c} T_0$ obtained by integrating the Doppler

measurement to the i-th satellite at time-step k, which represents the discrete-time instant $t_k = t_0 + kT_0$ for an initial time t_0, expressed in meters, is modeled as

$$\Phi_i(k) = \|\boldsymbol{r}_r - \boldsymbol{r}_{SV_i}(k')\|_2 + c \cdot [\delta t_r(k) - \delta t_{SV_i}(k')] + c \cdot [\delta t_{trop_i}(k) + \delta t_{iono_i}(k)] + \lambda_j N_i + \nu_i(k), \quad (22)$$

where $\boldsymbol{r}_r \triangleq [x_r, y_r, z_r]^\mathsf{T}$ is the stationary receiver's position vector in the East-North-Up (ENU) frame; $\boldsymbol{r}_{SV_i} \triangleq [x_{SV_i}, y_{SV_i}, z_{SV_i}]^\mathsf{T}$ is the i-th satellite's position vector in the ENU frame; δt_r and δt_{SV_i} are the receiver's and i-th satellite's clock biases, respectively; δt_{trop_i} and δt_{iono_i} are the ionospheric and tropospheric delays between the receiver and i-th satellite, respectively; c is the speed-of-light; λ_i is the wavelength of the i-th satellite's signal; N_i is the carrier phase ambiguity between the receiver and i-th satellite; and ν_i is the measurement noise, which is modeled as a discrete-time zero-mean white sequence with variance $\sigma^2_{\Phi,i}$. In (22), the time index k' represents discrete time-step $t_k = t_0 + kT_0 - \delta t_{TOF_i}$, where δt_{TOF_i} is the time-of-flight of the signal from the i-th satellite to the receiver. This paper assumes $k' \approx k$ to simplify the formulation of the NLS positioning framework. This approximation introduces an error in the LEO satellite position and clock bias. The error introduced by this approximation in the LEO satellite position is negligible compared to the position error in TLE files, which can be as high as few kilometers. The error introduced by this approximation in the LEO satellite clock will be lumped into a combined term and estimated as described next.

The receiver and LEO satellite clock error states (bias and drift) are modeled according to the standard double integrator model [3]. The terms $\delta t_r(k)$, $\delta t_{SV_i}(k)$, $\delta t_{iono_i}(k)$, $\delta t_{trop_i}(k)$ will be lumped together and approximated as a first-order TSE. Under these assumptions, (22) can be approximated as

$$\Phi_i(k) \approx \|\boldsymbol{r}_r - \boldsymbol{r}_{SV_i}(k)\|_2 + a_i + b_i k T_0 + \nu_i(k), \quad (23)$$

where $a_i \triangleq c \cdot (\delta t_r - \delta t_{SV_i} + \delta t_{iono_i} + \delta t_{trop_i})$ and $b_i \triangleq c \cdot \left(\dot{\delta} t_r - \dot{\delta} t_{SV_i} + \dot{\delta} t_{iono_i} + \dot{\delta} t_{trop_i}\right)$ are the zero- and first-order TSE terms, respectively, of the lumped clock errors and atmospheric delays.

B. Batch NLS Estimator

Next, define the state vector $\boldsymbol{x} \triangleq \left[\boldsymbol{r}_r{}^\mathsf{T}, a_1, b_1, \ldots, a_L, b_L\right]^\mathsf{T}$. Let $\boldsymbol{z}(k)$ denote the vector of carrier phase observables from all LEO satellites, available at time-step k, stacked together, i.e. $\boldsymbol{z}(k) \triangleq [\Phi_1(k), \ldots, \Phi_L(k)]^\mathsf{T}$. The vector of all available observables is defined as $\boldsymbol{z} \triangleq [\boldsymbol{z}(0), \ldots, \boldsymbol{z}(M)]^\mathsf{T}$, where M is the total number of observations during the satellite's pass. Let $\boldsymbol{v}_z$ denote the vector of all measurement noises stacked together. Then, one can readily write the measurement equation given by $\boldsymbol{z} = \boldsymbol{g}(\boldsymbol{x}) + \boldsymbol{v}_z$, where $\boldsymbol{g}(\boldsymbol{x})$ is the nonlinear mapping from the state space $\boldsymbol{x}$ to the measurement space $\boldsymbol{z}$. The positioning solution is achieved by iterating over the NLS update equation

$$\Delta\hat{\boldsymbol{x}}_p = \left(\mathbf{H}_p^\mathsf{T}\mathbf{H}_p\right)^{-1}\mathbf{H}_p^\mathsf{T}\left(\boldsymbol{z} - \mathbf{g}(\hat{\boldsymbol{x}}_p)\right),$$
$$\hat{\boldsymbol{x}}_{p+1} = \hat{\boldsymbol{x}}_p + \Delta\hat{\boldsymbol{x}}_p, \quad (24)$$

where $p \in \{1, 2, \ldots, p^*\}$ denotes the recursion index; p^* is the index when $\|\Delta\hat{\boldsymbol{x}}_p\|_2$ reaches a predetermined stopping criterion (chosen to be 10^{-6}); $\mathbf{H}_p \triangleq \frac{\partial \boldsymbol{g}(\boldsymbol{x})}{\partial \boldsymbol{x}}|_{\boldsymbol{x}=\hat{\boldsymbol{x}}_p}$ is the measurement Jacobian matrix.

C. Experimental Results

Signals from 1 Orbcomm, 1 Iridium NEXT, 4 Starlink, and 2 OneWeb LEO satellites were collected via the setup described in Fig. 3. Fig. 12(a) shows the skyplot of the LEO satellites, while Fig. 12(b) shows the hardware used for data collection. The hardware included: (i) an LNB with conversion gain of 50 dB and noise figure of 2.5 dB connected to a Ku-band 60 cm parabolic offset dish with gain of 30 dBi to receive Starlink and OneWeb satellite signals, (ii) a commercial Orbcomm antenna, and (iii) a commercial Iridium NEXT antenna. The satellite positions, $\{\boldsymbol{r}_{SV_i}\}_{i=1}^8$, were obtained from TLE files and an SGP4 orbit determination software. The TLE epoch time was adjusted for each satellite to account for ephemeris errors. This was achieved by minimizing the carrier phase residuals for each satellite [27]. The blind Doppler tracking framework discussed in III was used to acquire and track satellite signals with $q_w = (0.1)^2$ rad^2/s^6 and $\sigma_{\dot{\theta}} = \frac{\pi}{6}$ rad/s. Results of 8 different satellites are shown in Fig. 11. Note that cut-offs in Doppler tracking for OneWeb and Starlink are caused by the inability to continuously point the highly directional dish manually towards the satellite position. The top graphs in the figure show the estimated (dashed) versus the TLE+SGP4-predicted (solid) Doppler shift profile for every tracked satellite. The bottom graphs show the KF innovation $\nu_{KF}(k)$ during the tracking period. It is worth noting that even though the studied LEO constellations suffer from high Doppler (up to ∼250 kHz), the blind Doppler tracking framework was able to track the Doppler with an error less than 10 Hz.

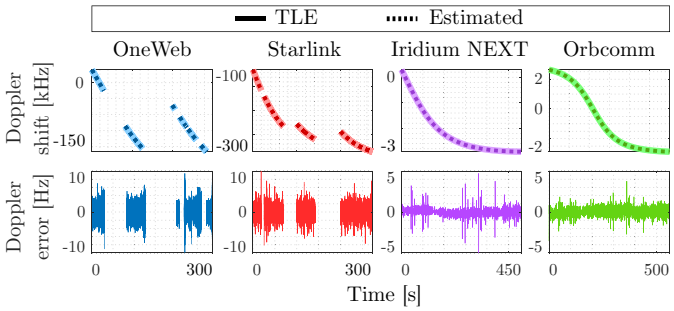

Fig. 11. Top: Doppler shift profiles for 2 OneWeb, 4 Starlink, 1 Iridium NEXT, and 1 Orbcomm LEO satellites: solid curves denote the estimated Doppler from the proposed framework, while dotted curves denote the predicted Doppler from TLE+SGP4. Bottom: KF innovation during the tracking period of each satellite.

Next, the batch NLS estimator described in (24) was employed using measurements from all LEO satellites to obtain the final estimate $\hat{\boldsymbol{x}}_{p^*}$. The receiver's initial position estimate, $\hat{\boldsymbol{r}}_{r,0}$, was set on the roof of the Engineering parking structure at the University of California, Irvine, USA, approximately 3,600 km away from the true position, which was on the roof of The Ohio State University's Electroscience Laboratory (ESL), Columbus, Ohio, USA. Fig. 13 summarizes the positioning

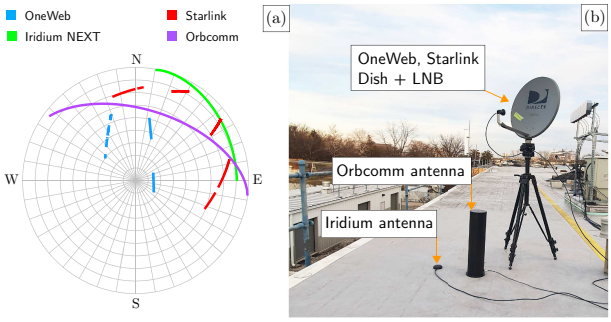

Fig. 12. (a) Skyplot of 2 OneWeb, 4 Starlink, 1 Iridium NEXT, and 1 Orbcomm LEO satellites which were tracked during the experiment. (b) Hardware setup used in data collection.

results. Specifically, Fig. 13(a) shows the trajectories of the 8 satellites from the 4 LEO constellations, Fig. 13(b) shows the initial and final position estimates, and Fig. 13(c) shows the true and estimated receiver's position. The final 3–D position error was found to be 5.8 m, while the 2–D position error was 5.1 m (i.e., upon considering only the east and north coordinates in the ENU frame). For comparative purposes, the batch NLS estimator was employed with the individual LEO constellations. The results are summarized in Table II.

IX. Conclusion

This paper proposed a novel framework for blind beacon estimation and Doppler tracking of LEO satellites. First, it provided a derivation of an analytical expression for the received signal frequency spectrum. Second, a novel frequency-based Doppler discriminator was proposed. Third, a KF-based Doppler tracking algorithm was developed. Fourth, a blind beacon estimation framework was proposed and demonstrated with four LEO constellations, namely, Orbcomm, Iridium NEXT, Starlink, and OneWeb. Finally, the paper showed the first result of stationary receiver localization with multi-constellation LEO satellite including OneWeb, achieving a 2–D position error of 5.1 m.

Acknowledgment

The authors would like to thank the Electroscience Laboratory (ESL) and Mr. Jeffrey Blankenship for his readiness and generous support in the experimental setup.

TABLE II
Comparison of positioning results with different LEO constellations

Constellation	Visibility [s]	2–D Error [m]
OneWeb	132	30.68
Starlink	215	33.69
Iridium NEXT	490	34.48
Orbcomm	560	31.57
All	560	5.1

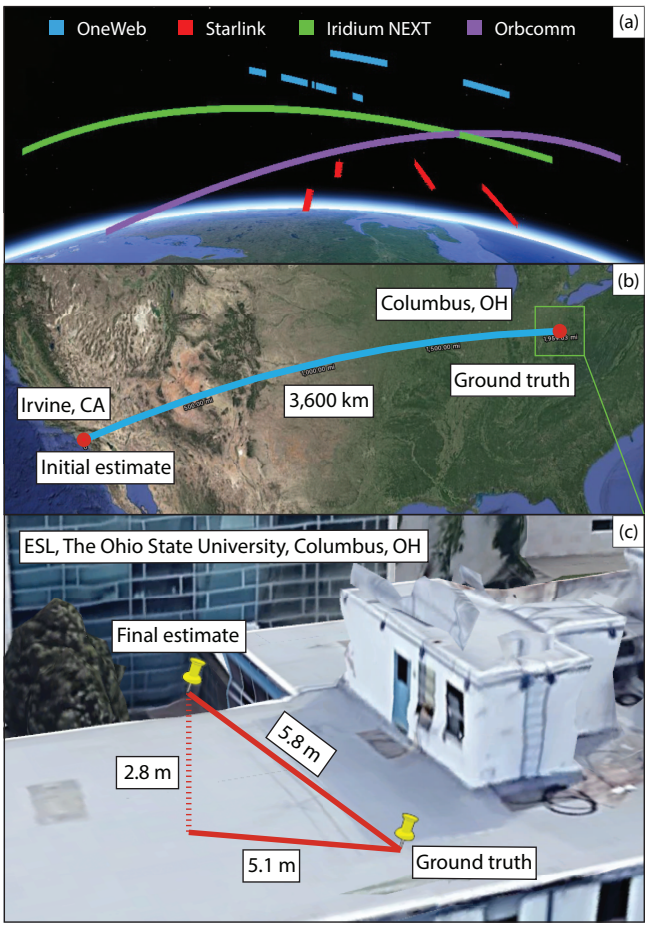

Fig. 13. Positioning results with 2 OneWeb, 4 Starlink, 1 Iridium NEXT, and 1 Orbcomm LEO satellites: (a) LEO satellite trajectories. (b) Initial and final estimated positions. (c) Final errors relative receiver's true position.

References

[1] G. Curzi, D. Modenini, and P. Tortora, "Large constellations of small satellites: A survey of near future challenges and missions," *Aerospace*, vol. 7, no. 9, pp. 1–18, September 2020.

[2] T. Reid, T. Walter, P. Enge, D. Lawrence, H. Cobb, G. Gutt, M. O'Conner, and D. Whelan, "Position, navigation, and timing technologies in the 21st century," J. Morton, F. van Diggelen, J. Spilker, Jr., and B. Parkinson, Eds. Wiley-IEEE, 2021, vol. 2, ch. 43: Navigation from low Earth orbit – Part 1: Concept, Current Capability, and Future Promise, pp. 1359–1379.

[3] Z. Kassas, "Position, navigation, and timing technologies in the 21st century," J. Morton, F. van Diggelen, J. Spilker, Jr., and B. Parkinson, Eds. Wiley-IEEE, 2021, vol. 2, ch. 43: Navigation from low Earth orbit – Part 2: models, implementation, and performance, pp. 1381–1412.

[4] R. Faragher, "Effects of multipath interference on radio positioning systems," Ph.D. dissertation, University of Cambridge, England, 2007.

[5] R. Ioannides, T. Pany, and G. Gibbons, "Known vulnerabilities of global navigation satellite systems, status, and potential mitigation techniques," *Proceedings of the IEEE*, vol. 104, no. 6, pp. 1174–1194, February 2016.

[6] X. Chen, Q. Wei, F. Wang, Z. Jun, S. Wu, and A. Men, "Super-resolution time of arrival estimation for a symbiotic FM radio data system," *IEEE Transactions on Broadcasting*, vol. 66, no. 4, pp. 847–856, December 2020.

[7] L. Chen, P. Thevenon, G. Seco-Granados, O. Julien, and H. Kuusniemi, "Analysis on the TOA tracking with DVB-T signals for positioning," *IEEE Transactions on Broadcasting*, vol. 62, no. 4, pp. 957–961, December 2016.

[8] R. Faragher and R. Harle, "Towards an efficient, intelligent, opportunistic smartphone indoor positioning system," *NAVIGATION, Journal of the Institute of Navigation*, vol. 62, no. 1, pp. 55–72, 2015.

[9] J. Khalife, K. Shamaei, and Z. Kassas, "A software-defined receiver architecture for cellular CDMA-based navigation," in *Proceedings of IEEE/ION Position, Location, and Navigation Symposium*, April 2016, pp. 816–826.

[10] C. Yang, T. Nguyen, and E. Blasch, "Mobile positioning via fusion of mixed signals of opportunity," *IEEE Aerospace and Electronic Systems Magazine*, vol. 29, no. 4, pp. 34–46, April 2014.

[11] J. del Peral-Rosado, J. López-Salcedo, F. Zanier, and G. Seco-Granados, "Position accuracy of joint time-delay and channel estimators in LTE networks," *IEEE Access*, vol. 6, pp. 25 185–25 199, 2018.

[12] K. Shamaei and Z. Kassas, "A joint TOA and DOA acquisition and tracking approach for positioning with LTE signals," *IEEE Transactions on Signal Processing*, pp. 2689–2705, 2021.

[13] A. Xhafa, J. del Peral-Rosado, J. López-Salcedo, and G. Seco-Granados, "Evaluation of 5G positioning performance based on UTDoA, AoA and base-station selective exclusion," *Sensors*, vol. 22, no. 1, pp. 101–118, 2021.

[14] A. Abdallah, J. Khalife, and Z. Kassas, "Exploiting on-demand 5G downlink signals for opportunistic navigation," *IEEE Signal Processing Letters*, vol. 30, no. 389–393, 2023.

[15] J. Peral-Rosado, J. Lopez-Salcedo, S. Kim, and G. Seco-Granados, "Feasibility study of 5G-based localization for assisted driving," in *Proceedings of International Conference on Localization and GNSS*, June 2016, pp. 1–6.

[16] M. Maaref, J. Khalife, and Z. Kassas, "Lane-level localization and mapping in GNSS-challenged environments by fusing lidar data and cellular pseudoranges," *IEEE Transactions on Intelligent Vehicles*, vol. 4, no. 1, pp. 73–89, March 2019.

[17] Z. Kassas, A. Abdallah, C. Lee, J. Jurado, J. Duede, Z. Hoeffner, T. Hulsey, R. Quirarte, S. Wachtel, and R. Tay, "Protecting the skies: GNSS-less accurate aircraft navigation with terrestrial cellular signals of opportunity," in *Proceedings of ION GNSS Conference*, September 2022, pp. 1014–1025.

[18] J. Del Peral-Rosado, P. Nolle, S. Razavi, G. Lindmark, D. Shrestha, F. Gunnarsson, F. Kaltenberger, N. Sirola, O. Särkkä, J. Roström, K. Vaarala, P. Miettinen, G. Pojani, L. Canzian, H. Babaroglu, E. Rastorgueva-Foi, J. Talvitie, and D. Flachs, "Design considerations of dedicated and aerial 5G networks for enhanced positioning services," in *Proceedings of Workshop on Satellite Navigation Technology*, April 2022, pp. 1–12.

[19] J. Khalife and Z. Kassas, "On the achievability of submeter-accurate UAV navigation with cellular signals exploiting loose network synchronization," *IEEE Transactions on Aerospace and Electronic Systems*, vol. 58, no. 5, pp. 4261–4278, October 2022.

[20] Z. Kassas, J. Khalife, A. Abdallah, and C. Lee, "I am not afraid of the GPS jammer: resilient navigation via signals of opportunity in GPS-denied environments," *IEEE Aerospace and Electronic Systems Magazine*, vol. 37, no. 7, pp. 4–19, July 2022.

[21] N. Jardak and Q. Jault, "The potential of LEO satellite-based opportunistic navigation for high dynamic applications," *Sensors*, vol. 22, no. 7, pp. 2541–2565, 2022.

[22] F. Farhangian, H. Benzerrouk, and R. Landry, "Opportunistic in-flight INS alignment using LEO satellites and a rotatory IMU platform," *Aerospace*, vol. 8, no. 10, pp. 280–281, 2021.

[23] M. Psiaki, "Navigation using carrier Doppler shift from a LEO constellation: TRANSIT on steroids," *NAVIGATION, Journal of the Institute of Navigation*, vol. 68, no. 3, pp. 621–641, September 2021.

[24] K. Wang and A. El-Mowafy, "LEO satellite clock analysis and prediction for positioning applications," *Geo-spatial Information Science*, vol. 25, no. 1, pp. 14–33, 2022.

[25] M. Hartnett, "Performance assessment of navigation using carrier Doppler measurements from multiple LEO constellations," Master's thesis, Air Force Institute of Technology, Ohio, USA, 2022.

[26] P. Iannucci and T. Humphreys, "Fused low-Earth-orbit GNSS," *IEEE Transactions on Aerospace and Electronics Systems*, 2022, accepted.

[27] J. Khalife, M. Neinavaie, and Z. Kassas, "The first carrier phase tracking and positioning results with Starlink LEO satellite signals," *IEEE Transactions on Aerospace and Electronic Systems*, vol. 56, no. 2, pp. 1487–1491, April 2022.

[28] Z. Kassas, M. Neinavaie, J. Khalife, N. Khairallah, J. Haidar-Ahmad, S. Kozhaya, and Z. Shadram, "Enter LEO on the GNSS stage: Navigation with Starlink satellites," *Inside GNSS Magazine*, vol. 16, no. 6, pp. 42–51, 2021.

[29] J. Khalife and Z. Kassas, "Performance-driven design of carrier phase differential navigation frameworks with megaconstellation LEO satellites," *IEEE Transactions on Aerospace and Electronic Systems*, vol. 1–20, 2023, accepted.

[30] C. Zhao, H. Qin, N. Wu, and D. Wang, "Analysis of baseline impact on differential doppler positioning and performance improvement method for LEO opportunistic navigation," *IEEE Transactions on Instrumentation and Measurement*, pp. 1–10, 2023.

[31] Z. Kassas, J. Morales, and J. Khalife, "New-age satellite-based navigation – STAN: simultaneous tracking and navigation with LEO satellite signals," *Inside GNSS Magazine*, vol. 14, no. 4, pp. 56–65, 2019.

[32] D. Shen, J. Lu, G. Chen, E. Blasch, C. Sheaff, M. Pugh, and K. Pham, "Methods of machine learning for space object pattern classification," in *Proceedings of IEEE National Aerospace and Electronics Conference*, 2019, pp. 565–572.

[33] J. Haidar-Ahmad, N. Khairallah, and Z. Kassas, "A hybrid analytical-machine learning approach for LEO satellite orbit prediction," in *Proceedings of International Conference on Information Fusion*, 2022, pp. 1–7.

[34] N. Khairallah and Z. Kassas, "An interacting multiple model estimator of LEO satellite clocks for improved positioning," in *Proceedings of IEEE Vehicular Technology Conference*, 2022, pp. 1–5.

[35] S. Kozhaya and Z. Kassas, "Blind receiver for LEO beacon estimation with application to UAV carrier phase differential navigation," in *Proceedings of ION GNSS Conference*, 2022, pp. 2385–2397.

[36] M. Neinavaie, J. Khalife, and Z. Kassas, "Acquisition, Doppler tracking, and positioning with Starlink LEO satellites: First results," *IEEE Transactions on Aerospace and Electronic Systems*, vol. 58, no. 3, pp. 2606–2610, June 2022.

[37] H. Choi and H. Moon, "Blind estimation of spreading sequence and data bits in direct-sequence spread spectrum communication systems," *IEEE Access*, vol. 8, pp. 148 066–148 074, 2020.

[38] Z. Rui, X. Ouyang, F. Zeng, and X. Xu, "Blind estimation of GPS M-Code signals under noncooperative conditions," *Wireless Communications and Mobile Computing*, vol. 2022, 2022.

[39] J. Khalife, M. Neinavaie, and Z. Kassas, "Blind Doppler tracking from OFDM signals transmitted by broadband LEO satellites," in *Proceedings of IEEE Vehicular Technology Conference*, April 2021, pp. 1–5.

[40] C. Zhao, H. Qin, and Z. Li, "Doppler measurements from multiconstellations in opportunistic navigation," *IEEE Transactions on Instrumentation and Measurement*, vol. 71, pp. 1–9, 2022.

[41] C. Huang, H. Qin, C. Zhao, and H. Liang, "Phase - time method: Accurate Doppler measurement for Iridium NEXT signals," *IEEE Transactions on Aerospace and Electronic Systems*, vol. 58, no. 6, pp. 5954–5962, 2022.

[42] T. Frederick, "Time-frequency estimation for cyclostationary signals," Ph.D. dissertation, Florida Atlantic University, USA, 1997.

[43] S. Vaseghi, *Advanced digital signal processing and noise reduction*. John Wiley & Sons, 2008.

[44] S. Zucker, "Cross-correlation and maximum-likelihood analysis: a new approach to combining cross-correlation functions," *Monthly Notices of the Royal Astronomical Society*, vol. 342, no. 4, pp. 1291–1298, 2003.

[45] 3GPP2, "Physical layer standard for cdma2000 spread spectrum systems (C.S0002-E)," 3rd Generation Partnership Project 2 (3GPP2), TS C.S0002-E, June 2011.

[46] A. Flores, "NAVSTAR GPS space segment/navigation user interfaces," https://www.gps.gov/technical/icwg/IS-GPS-200N.pdf, August 2022.

[47] R. Hendrickson, "Globalstar for the military," in *Proceedings of IEEE Military Communications Conference*, vol. 3, November 1997, pp. 1173–1178.

[48] 3GPP, "Evolved universal terrestrial radio access (E-UTRA); multiplexing and channel coding," 3rd Generation Partnership Project (3GPP), TS 36.212, January 2010. [Online]. Available: http://www.3gpp.org/ftp/Specs/html-info/36212.htm

[49] 3GPP, "Physical channels and modulation," https://www.etsi.org/deliver/etsi-ts/138200-138299/138211/15.02.00-60/ts-138211v150200p.pdf, 5G; NR; 3rd Generation Partnership Project (3GPP), TS 38.211, July 2018.

[50] S. Reid, "ORBCOMM system overview," December 2001.

[51] Orbcomm, "Ever wondered what is on the Orbcomm satellite downlink?" http://mdkenny.customer.netspace.net.au/Orbcomm.pdf, 2002.

[52] M. Nezami, "DSP-based carrier acquisition and tracking for burst TDMA mobile land and satellite receivers," *Applied Microwave & Wireless Magazine*, vol. 13, no. 9, pp. 24–41, 2001.